Available online at www.sciencedirect.com
ScienceDirect
Geochimica et Cosmochimica Acta 70 (2006) 5455–5468
Geochimica
www.elsevier.com/locate/gca

Sedimentary iron geochemistry in acidic waterways associated with coastal lowland acid sulfate soils

Edward D. Burton *, Richard T. Bush, Leigh A. Sullivan

Centre for Acid Sulfate Soil Research, School of Environmental Science and Management, Southern Cross University, Lismore, NSW 2480, Australia

Received 8 May 2006; accepted in revised form 17 August 2006

Abstract

We examined the solubility, mineralogy and geochemical transformations of sedimentary Fe in waterways associated with coastal lowland acid sulfate soils (CLASS). The waterways contained acidic (pH 3.26–3.54), Fe^{III}-rich (27–138 μM) surface water with low molar $Cl:SO_4$ ratios (0.086–5.73). The surficial benthic sediments had high concentrations of oxalate-extractable Fe(III) due to schwertmannite precipitation (kinetically favoured by 28–30% of aqueous surface water Fe being present as the $Fe^{III}SO_4^+$ species). Subsurface sediments contained abundant pore-water HCO_3 (6–20 mM) and were reducing (Eh < -100 mV) with pH 6.0–6.5. The development of reducing conditions caused reductive dissolution of buried schwertmannite and goethite (formed via in situ transformation of schwertmannite). As a consequence, pore-water Fe^{II} concentrations were high (>2 mM) and were constrained by precipitation–dissolution of siderite. The near-neutral, reducing conditions also promoted SO_4-reduction and the formation of acid-volatile sulfide (AVS). The results show, for the first time for CLASS-associated waterways, that sedimentary AVS consisted mainly of disordered mackinawite. In the presence of abundant pore-water Fe^{II}, precipitation–dissolution of disordered mackinawite maintained very low (i.e. <0.1 μM) S^{-II} concentrations. Such low concentrations of S^{-II} caused slow rates for conversion of disordered mackinawite to pyrite, thereby resulting in relatively low concentrations of pyrite (<300 μmol g^{-1} as Fe) compared to disordered mackinawite (up to 590 μmol g^{-1} as Fe). This study shows that interactions between schwertmannite, goethite, siderite, disordered mackinawite and pyrite control the geochemical behaviour of sedimentary Fe in CLASS-associated waterways.

1. Introduction

Acid sulfate waters are produced primarily as a result of the oxidation of pyrite and other sulfide minerals (such as pyrrhotite, marcasite and mackinawite) in rocks, soils and sediments (Bigham and Nordstrom, 2000). The formation of acid sulfate waters associated with coal or sulfide ore mining has received considerable attention. As a result, acid mine drainage (AMD) is probably the most widely known source of acid sulfate waters. In AMD environments, the geochemical cycling of Fe has been studied intensively and is known to be of great significance as a regulator of pH and contaminant mobility (e.g. Bigham et al., 1990; Meier et al., 2004; Regenspurg et al., 2004; Gammons et al., 2005).

In contrast to AMD settings, Fe geochemistry in acid sulfate waters associated with coastal lowland acid sulfate soils (CLASS) has received comparatively little research. These soils underlie approximately 20 million hectares of low-lying coastal land worldwide and are characterized by the presence of sulfidic subsoils (van Breemen, 1982; Dent, 2000). The sulfide mineralogy in CLASS is dominated by pyrite formed during the Holocene, but may in some locations include significant quantities of marcasite or greigite (Bush and Sullivan, 1997; Fanning et al., 2002; Bush et al., 2004a). Engineered drainage systems often represent a significant component of CLASS floodplain hydrology (Sammut et al., 1996; Astrom and Spiro, 2000). CLASS drains are designed to lower the water-table in order to

* Corresponding author. Fax: +61 2 6621 2669.
E-mail address: ed.burton@scu.edu.au (E.D. Burton).

0016-7037/$ - see front matter © 2006 Elsevier Inc. All rights reserved.
doi:10.1016/j.gca.2006.08.016

permit year-round agriculture. This promotes sulfide oxidation within the soil profile and thereby contributes to the formation of Fe-rich, acid sulfate ground-water and surface-water (Dent, 1986; Wilson et al., 1999; Ward et al., 2004).

Iron cycling in benthic sediments is known to influence surface water quality in many AMD environments. For example, schwertmannite-rich sediments control pH and Fe flux across the sediment–water interface in several AMD-affected lakes (Peine et al., 2000; Regenspurg et al., 2004). Available data indicate that schwertmannite may also be an important component of the sedimentary Fe cycle in CLASS drains (Sullivan and Bush, 2004). However unlike AMD environments where schwertmannite has been previously observed, CLASS drains typically contain abundant labile organic material due to dense growth of aquatic macrophytes (Smith and Melville, 2004; Burton et al., 2006a). This results in the accretion of organic-rich benthic sediments, characterized by a yellow-orange surface layer overlying soft gels (water content >90%) having a black "oily" appearance (Sullivan and Bush, 2000; Sullivan et al., 2002; Bush et al., 2004b; Smith and Melville, 2004).

Sullivan and Bush (2000) showed that the abundance of sedimentary acid-volatile sulfide (AVS; assumed to represent an amorphous $FeS_{(s)}$ phase) in CLASS drains can greatly exceed levels reported from other environments. The widespread, anomalous abundance of sedimentary AVS in such waterways has been further documented by Bush et al. (2004b), Smith and Melville (2004), Macdonald et al. (2004) and Burton et al. (2006a). Recent research has also examined the oxidative transformations of AVS during flood-induced sediment resuspension events in CLASS drains (Burton et al., 2006b). However, the geochemical transformations regulating the in situ sedimentary Fe mineralogy and solubility during the prevailing low flow, quiescent conditions in such waterways have not been addressed. As a consequence, the current understanding of Fe cycling in CLASS landscapes is incomplete and hinders the development of water quality management strategies.

The objective of this study was to determine the in situ solubility, mineralogy and geochemical cycling of sedimentary Fe during periods of sediment accretion in acidic CLASS drains. In particular, this study identifies for the first time the key mineral species and their geochemical transformations controlling sedimentary Fe accretion in such waterways.

2. Methods

2.1. Environmental setting and study sites

CLASS landscapes in many parts of the world are characterized by the presence of lowlying, sulfidic subsoil horizons which are, or have the potential to become, highly acidic due to sulfide oxidation (van Breemen, 1982; Dent, 2000; Fanning et al., 2002). Sulfide oxidation in these soils produces both protonic acidity as well as potential acidity associated with Fe^{II} oxidation and subsequent Fe^{III} hydrolysis (Ward et al., 2004). The release of CLASS oxidation products into nearby waterways contributes to the development of acid sulfate waters (van Breemen, 1982; Sammut et al., 1996; Astrom and Spiro, 2000; Johnston et al., 2004).

CLASS-landscapes are generally flood-prone and have therefore been widely modified through the construction of intensive drainage networks. CLASS drains mitigate the adverse effects of flooding and represent a significant component of the floodplain hydrology (Sammut et al., 1996). We examined Fe geochemistry in the benthic sediments of drains (termed sites T, S and B) situated on the floodplains of three major river systems in eastern Australia (Fig. 1). Site T (28°57′S, 153°23′E) was within the Tuckean Nature Reserve Drain on the Richmond River floodplain, site B (28°19′S, 153°26′E) was within Black's Drain on the Tweed River floodplain, and site S (29°30′S, 153°15′E) was within Maloney's Drain on the Clarence River floodplain. All three sites were unlined drains (5–8 m wide; 2–3 m deep) with floodgates or weirs to maintain a constant water level and prevent tidal flooding of the surrounding low-lying (<1 m above average sea-level) land.

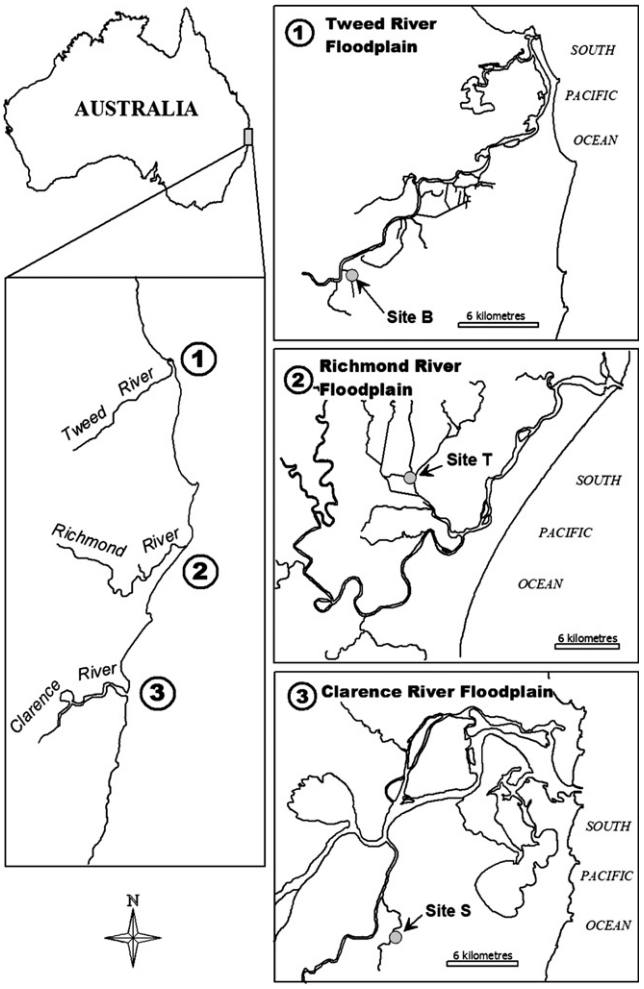

Fig. 1. Location of CLASS drain sites B, T and S described in this study.

The soils surrounding the study sites are typical of drained CLASS from eastern Australia (Fig. 2). Detailed profile descriptions are presented for soils near site T by Bush and Sullivan (1997, 1999), site B by Kinsela and Melville (2004) and Wilson et al. (1999), and site S by Johnston et al. (2004). The non-sulfidic surface soil layers extend to a depth of approximately 0.3 m and are composed of fluvially deposited sediment with pH 4–6. Below this surface layer is a sulfuric horizon, characterized by pH < 4 due to sulfuric acid produced via drainage-induced oxidation of sulfide minerals. The sulfuric horizon varies in depth from 0.5 to 1 m and exhibits high concentrations of soluble Fe (~0.1–2 mM) and SO_4 (~2–100 mM) (Johnston et al., 2004; Kinsela and Melville, 2004). The surface soil and sulfuric horizon overlie several metres (>8 m) of neutral (pH ~7) sulfidic clay gel with a pyrite content of 1–4% (Fig. 2). The sulfuric and sulfidic horizons were originally deposited as estuarine sediments during the Holocene (Dent, 2000).

The hydraulic conductivity of the oxidized sulfuric horizon (~10^{-1} to 10^{2} m day^{-1}) greatly exceeds that of the underlying sulfidic gel (<10^{-3} m day^{-1}) (Johnston et al., 2004). The three drains described here extend to depths of approximately 1–1.5 m into the lower sulfidic soil horizon. As a consequence, inputs of Fe-rich groundwater to these waterways occur mainly through the sides of the drains via the sulfuric horizon (Fig. 2). This important hydraulic feature means that solute advection through the benthic sediments is negligible.

The study sites experience mild, dry conditions during winter and spring (June–October) and warm, humid conditions during summer and autumn (November–May). The presence of flood-gates result in the study sites experiencing negligible surface-water flow for most of the year (Sammut et al., 1996). Dry weather in winter further contributes to stagnating flow conditions, thereby allowing accretion of fine sediments. Sediment resuspension is known to occur infrequently during short-lived flood-events in summer (Bush et al., 2004c).

2.2. Sample collection

Sample collection was performed in July, 2005 during a period of extended (several months of below average rainfall) dry weather. At the time of sample collection, the study sites contained 0.5–1.0 m of clear, stagnant surface water. Surface-water samples were collected mid-morning and stored on ice in acid-cleaned polypropylene containers with zero head-space prior to further processing (which commenced within 2 h). A 50 mL syringe was used to withdraw near-surface sediment (0–1 cm depth segment) for characterization of mineralogy. Sediment cores (internal diameter of 10 cm) were retrieved using a push-tube coring device. The intact cores were extruded step-wise from the corer and were incrementally sectioned into 2 or 4 cm intervals. As the core was extruded, sediment from each depth interval was directly transferred into 50 mL polypropylene vials (this was completed in less than 1–2 min for each depth interval). The vials were completely filled with sediment (no bubbles or headspace) and sealed with gas-tight screw-caps. Possible oxidation of reduced species was minimized by rapid sediment sectioning, avoidance of unnecessary sediment disturbance, and by transporting the sediment-filled vials on ice under an N_2 atmosphere.

2.3. Aqueous-phase properties

The pH and redox potential (Eh) of surface water samples were determined in the field. Sediment pore-water was extracted, within 24 h of sediment collection, by centrifugation (2000*g*, 20 min) of the sediment-filled 50 mL vials used to store the samples during transport. Surface- and pore-water samples were filtered to <0.45 μm using enclosed syringe-driven filter units (to minimize atmospheric exposure). Pore-water S^{-II}, which include H_2S, HS^-, S^{2-} and aqueous FeS complexes/clusters, were preserved with ZnOAc prior to determination by the methylene blue method (APHA, 1998). Aliquots of filtrate were added to 1,10-phenanthro-

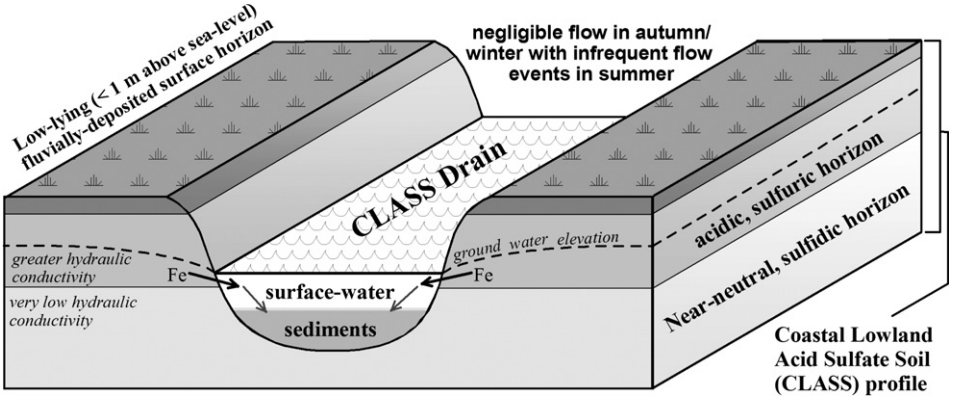

Fig. 2. Environmental setting of the flood-gated CLASS drain sites described in this study. We examined Fe geochemistry in the benthic sediments of three such waterways during periods of sediment accretion.

line solutions for Fe(II) determination (APHA, 1998). Alkalinity was determined by titration with 0.01 M HCl using the Gran procedure (Stumm and Morgan, 1996). Calcium, K, Mg, Na, SO_4 and Fe_{Total} were determined by inductively coupled plasma-atomic emission spectrometry (ICP-AES). Chloride was determined by the automated mercuric-thiocyanate method (APHA, 1998). For all aqueous parameters, triplicate determinations on 25% of samples revealed analytical precision within 5%. Calculation of the sum of cationic and anionic charge generally indicated acceptable charge balance (surface water at site B and site S and all pore-water data <10% error, mostly <3% error). Surface water at site T exhibited a significant charge imbalance due to an excess of quantified anions over cations, which may be attributed to the presence of high concentrations of cations other than those quantified (i.e. Ca, Mg, Na and K).

Activity coefficients for aqueous species were calculated by the Davies equation using PHREEQC 2.11 (Parkhurst and Appelo, 1999). Saturation index (*SI*) values for selected Fe minerals were calculated using the Minteq database (updated with recent thermodynamic data from Majzlan et al., 2004).

2.4. Solid-phase properties

Sediment pH, Eh and moisture content were determined as described by Burton et al. (2005). Organic carbon content (carbonates removed with 6 M HCl) was determined using a LECO-CNS 2000 induction furnace analyzer. Solid-phase reduced inorganic S (RIS) species were determined by a 3-step sequential extraction procedure. Acid-volatile sulfide (AVS) was extracted using the method of Hsieh et al. (2002), which involves the use of ascorbic acid to prevent Fe(III) interferences. The sediment slurry remaining after AVS extraction was transferred to an acetone-washed 50 mL vial, centrifuged (4000*g*, 30 min) and the supernatant discarded. Elemental S ($S^0_{(s)}$) was extracted by shaking the residual sediment with 20 mL of acetone for 24 h (Wieder et al., 1985), followed by a further 10 mL acetone rinse. The acetone-sediment slurry was separated by centrifugation (4000*g*, 10 min) and the supernatant acetone phase was transferred to a 250 mL conical flask. The acetone extract was dried under a stream of N_2 and $S^0_{(s)}$ extracted from the dry residue by Cr-reduction (Sullivan et al., 2000). Pyrite-S was then extracted from the AVS- and $S^0_{(s)}$ -extracted sediment also by Cr-reduction (Sullivan et al., 2000). The quantity of S, corresponding to each of the three RIS species, was determined via iodometric titration.

Total Fe concentrations were determined by aqua-regia digestion (1:3 HNO_3:HCl, 20 min, 1000 W microwave at 10% power) followed by ICP-AES analysis. Reactive solid-phase Fe(II) and Fe(III) were recovered by anoxic oxalate extraction and analysed by the 1,10-phenanthroline method (Phillips and Lovley, 1987; APHA, 1998). This procedure extracts Fe(II) from $FeS_{(s)}$ and $FeCO_{3(s)}$ as well as Fe(II)/Fe(III) from amorphous to crystalline (oxy)hydroxides. When performed under anoxic conditions, the oxalate extraction procedure does not alter the oxidation state of the extracted Fe (Phillips and Lovley, 1987).

Sediment samples were freeze-dried and examined by X-ray powder diffraction (XRPD) and scanning electron microscopy (SEM). X-ray diffractograms were obtained for randomly oriented powders using a Phillips PW 1050/70 diffractometer with a Cu X-ray tube. Samples were step scanned from 5°2θ to 65°2θ using a 0.05°2θ step and a 4 s count time. Samples for SEM examination were mounted on aluminium stubs, coated with carbon, and the elemental composition and morphology of selected specimens determined using a Leica 440 SEM with an ISIS energy dispersive X-ray (EDX) microanalysis system, utilizing a peak-to-background method (Sullivan and Bush, 1997).

2.5. General methods

All laboratory glass- and plastic-ware was cleaned by soaking in 5% (v/v) HNO_3 for at least 24 h, followed by repeated rinsing with deionised water. All chemicals were analytical reagent grade, and all reagent solutions were prepared with deionised water (milliQ). Deoxygenated solutions were prepared by purging with N_2 for at least 2 h.

In the present study, total aqueous concentrations are presented without valence (e.g. Fe and SO_4), individual aqueous species are shown with a charge (e.g. $Fe(OH)^{2+}$ and CO_3^{2-}) and the sum of aqueous species for components with a specific redox state are indicated by superscripted Roman numerals (e.g Fe^{II} and S^{-II}). The sum of solid-phase species for components with a specific redox state are indicated by upper-case Roman numerals (e.g. Fe(III) and S(−II)) All solid-phase results are presented on a dry weight basis.

3. Results and discussion

3.1. Surface-water properties

Surface-water at the three study sites was acidic, spanning pH 3.26–3.54 (Table 1). Sites T and B were essentially

Table 1
Selected properties for surface water at sites T, S and B

	Site T	Site S	Site B
pH	3.54	3.48	3.26
Na	1.51	99.8	1.82
K	0.013	1.72	0.12
Ca	0.27	2.18	0.36
Mg	0.34	12.4	0.73
SO_4	5.48	18.5	2.10
Cl	0.47	106	1.04
Al	0.064	0.022	0.340
Fe^{III}	0.072	0.138	0.027

Concentrations are expressed in mmol L^{-1}. The concentrations of total aqueous Fe and Fe^{III} differed by <5%, indicating that Fe^{II} was negligible.

freshwater systems with the Cl concentrations (Table 1) comprising <0.5% of average seawater Cl (545 mM; Stumm and Morgan, 1996). In contrast, site S was more typical of an estuarine waterway with the Cl concentration representing 19.4% of the Cl concentration in average seawater. The molar Cl:SO_4 ratios were 0.086 for site T, 5.73 for site S and 0.495 for site B, reflecting substantial enrichment in SO_4 compared with the corresponding ratio in average seawater (Cl:SO_4 = 19.3). Such low Cl:SO_4 ratios are typical for CLASS landscapes where widespread pyrite oxidation has released substantial quantities of SO_4 into groundwater (Johnston et al., 2004; Macdonald et al., 2004). This acid sulfate groundwater is known to discharge, via the sulfuric soil horizon, into the waterways described here (Johnston et al., 2004; Fig. 2).

The surface-water contained moderately high concentrations of aqueous Fe^{III} (27–138 μM), with <5% of total aqueous Fe as Fe^{II} (Table 1). Fig. 3 shows the equilibrium solubility of potential solid-phase Fe(III) species compared to the calculated Fe^{3+} activities in the acidic waterways described here. The calculated surface-water Fe^{3+} activities slightly exceeded the solubility windows for ferrihydrite and schwertmannite (Fig. 3). In contrast, the Fe^{3+} activities greatly exceeded the solubility of both goethite and jarosite by >3 orders of magnitude (Fig. 3). The supersaturated nature of the surface water suggests that precipitation of ferrihydrite, schwertmannite, goethite or jarosite may actively contribute to the accretion of benthic sediments.

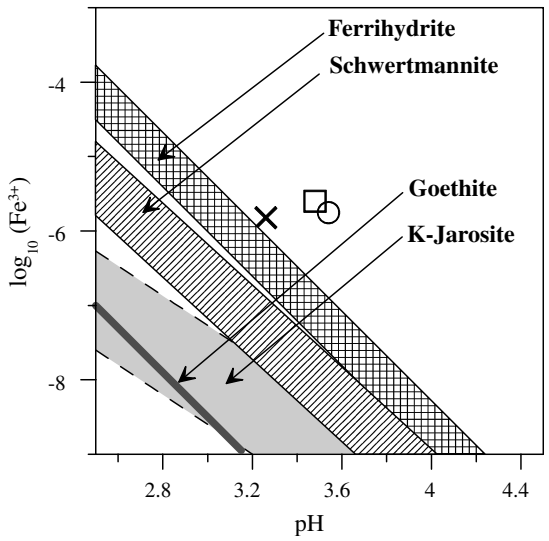

Fig. 3. Relationship between pH and Fe^{3+} activity for surface water from sites T (circle), S (square) and B (cross); in comparison to the pH-dependency of Fe^{3+} activities in equilibrium with potential Fe(III) solid-phases. Solubility windows for schwertmannite and jarosite are presented for 10^{-3} to 10^{-2} M SO_4^{2-} and 10^{-5} to 10^{-3} M K^+. The solubility lines are presented for solubility products of $(Fe^{3+})/(H^+)^3 = 10^{3.4 \pm 0.5}$ for two-line ferrihydrite (Majzlan et al., 2004), $(Fe^{3+})(OH^-)^3 = 10^{-41.5}$ for goethite (Parkhurst and Appelo, 1999), $(K^+)(Fe^{3+})^3\ (SO_4^{2-})^2/(H^+)^6 = 10^{-14.8}$ for jarosite (Parkhurst and Appelo, 1999), and $(Fe^{3+})^8(SO_4^{2-})/(H^+)^{22} = 10^{9.6 \pm 4}$ for schwertmannite (Majzlan et al., 2004).

The actual precipitation of ferrihydrite, schwertmannite, goethite and jarosite may be heavily influenced by kinetic constraints. Regenspurg et al. (2004) explain that the precipitation kinetics of these minerals are dependent on aqueous Fe speciation. Speciation calculations using PHREEQC showed that the $Fe^{III}SO_4^+$ species comprised 28–30% of total aqueous Fe, with 57–64% present as Fe^{III}-OH species in the three waterway study sites. Significant Fe^{III} ligation by SO_4 is thought to kinetically inhibit direct ferrihydrite and goethite precipitation, whereas ligation by OH^- inhibits direct jarosite precipitation (Regenspurg et al., 2004; Majzlan and Myneni, 2005). Therefore, the relative co-abundance of both Fe^{III}-OH and Fe^{III}-SO_4 species is expected to kinetically favour the initial precipitation of poorly ordered schwertmannite:

$$8Fe^{3+} + SO_4^{2-} + 14H_2O \rightleftharpoons Fe_8O_8(OH)_6(SO_4) + 22H^+ \quad (1)$$

The presence of schwertmannite was confirmed by XRPD for material from the sediment–water interface at sites T and S (Fig. 4). Examination of this material by SEM-EDX revealed that it exhibited "pin-cushion" morphology (Fig. 5a and b), which is consistent with previous reports for schwertmannite (Bigham et al., 1996; Sullivan and Bush, 2004).

3.2. General sediment properties

In contrast to the acidic surface-water, the sediment pore-water ranged from pH 6–6.5 at depth (Fig. 6). The Eh values for the 10–22 cm depth intervals were generally less than −100 mV (Fig. 6), which indicate anoxic reducing conditions. This is consistent with consumption of O_2 during degradation of abundant organic C (organic C contents were up to 9% at site T, 7% at site S and 7% at site B; Fig. 6). The pore-water HCO_3 concentrations increased with depth, attaining concentrations of 8.61 mM at site T, 19.7 mM at site S and 14.7 mM at site B (Fig. 6). In contrast, the pore-water SO_4 concentrations generally decreased with increasing sediment depth (Fig. 6). This is consistent with SO_4-reduction during degradation of simple organic molecules (e.g. lactic acid, $CH_3CHOHCOOH$; Langmuir, 1997):

$$2CH_3CHOHCOOH + SO_4^{2-} \rightarrow 2CH_3COOH + H_2S + 2HCO_3^- \quad (2)$$

The pore-water SO_4 concentrations approached the substrate saturation concentration for SO_4-reduction of 300 μM in the lower depth intervals (Ingvorsen et al., 1984). This indicates that the rate of SO_4-reduction may be limited by the lower pore-water SO_4 concentrations at depth.

The abundance of AVS spanning 307–405 μmol g^{-1} at site T, 308–590 μmol g^{-1} at site S and <1–309 μmol g^{-1} at site B are a result of SO_4-reduction (Fig. 7). These

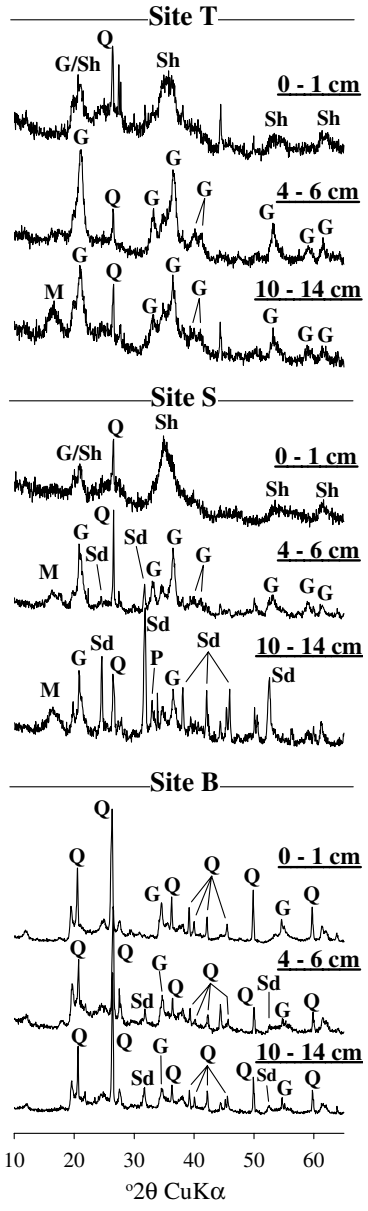

Fig. 4. Representative X-ray powder diffractograms for sediment samples from various depth intervals at sites T, S and B. G, goethite; M, disordered mackinawite; Q, quartz; P, pyrite; Sd, siderite and Sh, schwertmannite.

AVS concentrations are comparable with previous studies examining sediments from CLASS drains (Sullivan and Bush, 2000; Sullivan et al., 2002; Macdonald et al., 2004; Bush et al., 2004b; Burton et al., 2006a). However, they are high in comparison with sediments from natural estuarine and marine sediments, where AVS is typically present at <90 μmol g^{-1} (Morse and Cornwell, 1987; Burton et al., 2005).

3.3. Iron solubility in sediment pore-water

Pore-water Fe was dominantly the Fe^{II} species, with Fe^{III} comprising <5% of total aqueous Fe (i.e. less than the analytical precision of the Fe speciation method). This is consistent with the Eh results, which indicate that Fe(III) reduction is likely to be important in the anoxic sub-surface sediments described here (Lovley, 1997). The pore-water Fe^{II} concentrations were high, spanning 3–8 mM near the sediment surface, decreasing to 2–3 mM at greater depth (Fig. 8). Comparable concentrations of Fe^{II} have been reported in sub-oxic sediments of an AMD-affected lake (2–15 mM) underlying schwertmannite-rich surficial sediment (Peine et al., 2000). In comparison, pore-water Fe^{II} rarely exceeds 0.2 mM in marine sediments and 0.5 mM in Fe-rich salt-marsh sediments (e.g. Luther et al., 1992; Canfield et al., 1993; Neumann et al., 2005).

The pore-water S^{-II} concentrations were below detection (<1 μM) for all samples, thereby demonstrating that AVS was almost entirely composed of solid-phase S(−II) species. The undetectable pore-water S^{-II} concentrations described here can be attributed to the very high concentrations of pore-water Fe^{II} according to (Morse et al., 1987):

$$(HS^-) = \frac{K_{sp}10^{-pH}}{(Fe^{II})} \quad (3)$$

where K_{sp} denotes the solubility product constant, which equals $10^{-2.95}$ for amorphous $FeS_{(s)}$ (Morse et al., 1987). According to Eq. (3), pore-water S^{-II} would be expected to be maintained at <0.1 μM when in equilibrium with the high pore-water Fe^{II} concentrations and pH conditions reported here.

Pore-water Fe^{II} concentrations were similar at all three sites for sediment from depths greater than 10 cm below the sediment–water interface (i.e. 2–3 mM; Fig. 8). These concentrations are remarkably consistent with previously reported concentrations for the 10–22 cm depth interval in CLASS drain sediments (Fig. 8 presents data from Smith and Melville, 2004; and from Burton et al., 2006a). This consistency suggests that a specific process or phase may provide a general control on pore-water Fe^{II} solubility.

The high pore-water HCO_3 concentrations presented in Fig. 6 suggest that siderite ($FeCO_{3(s)}$) precipitation–dissolution may influence Fe^{II} solubility:

$$Fe^{2+} + HCO_3^- \rightleftharpoons FeCO_{3(s)} + H^+ \quad (4)$$

Fig. 9 demonstrates that most of the pore-water pH/Eh data lie within the stability field for siderite. These stability fields were calculated for 0.001 M Fe, 0.001 M SO_4 and 0.01–0.001 M HCO_3, which generally reflect the observed pore-water data (Figs. 6 and 9). A more direct indication of controls on Fe^{II} solubility for individual pore-water samples was determined by calculation of saturation index (SI) values for siderite:

$$SI = \log_{10}\frac{IAP}{K_{sp}} = \log_{10}\frac{(Fe^{2+})(CO_3^{2-})}{10^{-10.41}} \quad (5)$$

where K_{sp} and IAP denote the solubility product constant and ion activity product, respectively, for siderite. Fig. 10 shows that all three sites exhibited *SI* values for siderite spanning 1–1.5 for most of the depth intervals examined

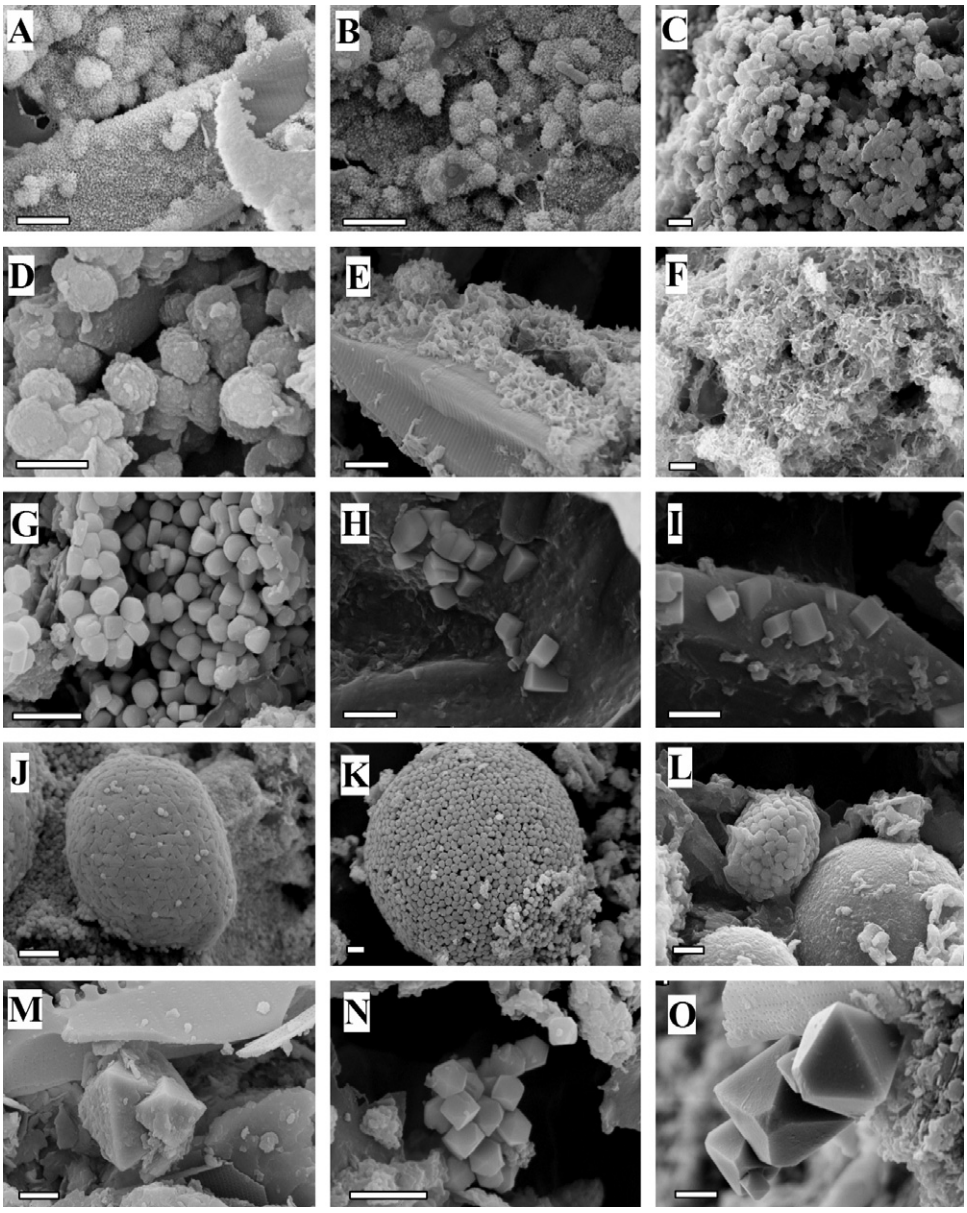

Fig. 5. Morphological features of important Fe minerals in CLASS drain sediments. A, B, schwertmannite; C, D, goethite; E, F, disordered mackinawite; G, H, I, siderite; J, K, L, framboidal pyrite and M, N, O, euhedral pyrite. The scale bar represents 2 μm. The identity of these minerals was verified according to their elemental composition as determined by EDX analysis and XRPD analysis of bulk samples.

(except surface sediment at site B, which was pH < 5). Comparable degrees of supersaturation have been reported in several field-based studies of siderite formation in non-CLASS settings (Postma, 1982; Bjerg et al., 1995; Amirbahman et al., 1998; Jakobsen and Postma, 1999).

The magnitude and uniformity in the *SI* values for siderite suggest that precipitation/dissolution of this phase may regulate pore-water Fe^{II} concentrations. The apparent supersaturation reflected in $SI > 0$ may be partly due to slow rates of siderite precipitation. Jensen et al. (2002) found that precipitation of siderite from supersaturated solutions required longer than 474 days to attain $SI = 0$ (i.e. equilibrium). However, these researchers also found that relatively rapid siderite precipitation resulted in *SI* values spanning 1–2 within approximately 15 days. This demonstrates that, in Fe^{II}- and HCO_3-rich solutions, siderite precipitation readily produces *SI* values that are consistent with Fig. 10 and such *SI* values persist for long periods (i.e. >450 days; Jensen et al., 2002).

3.4. Solid-phase Fe properties

Total Fe concentrations spanned 404–7440 μmol g^{-1} at site T, 3990–6240 μmol g^{-1} at site S and 613–2290 μmol g^{-1} at site B (Fig. 11). A substantial proportion of total Fe was recovered by oxalate extraction, with

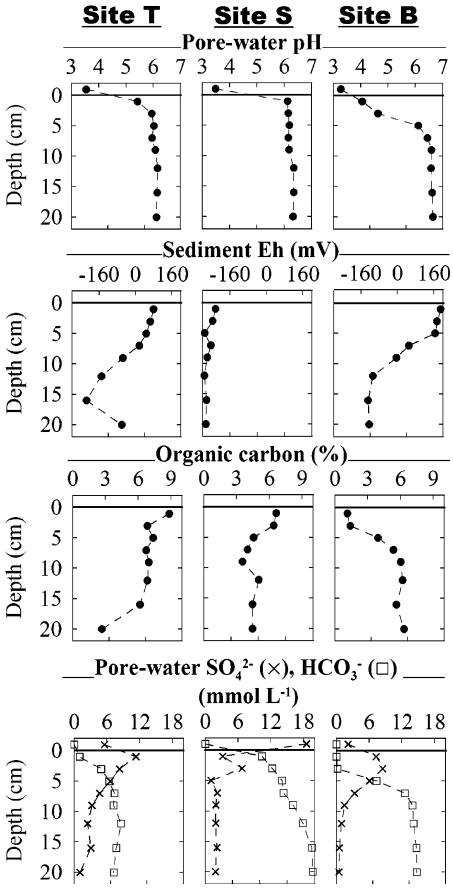

Fig. 6. Selected properties of sediment profiles collected from sites T, S and B.

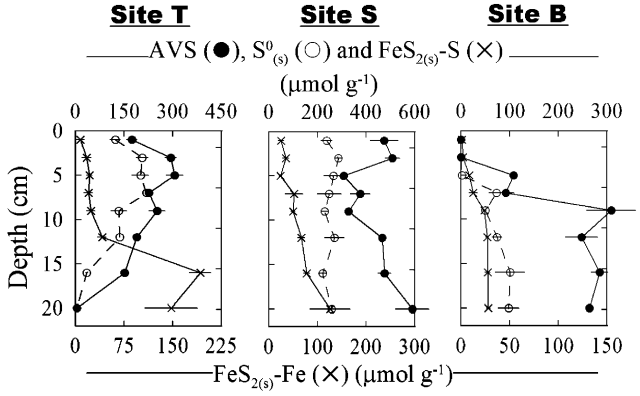

Fig. 7. Reduced inorganic S (RIS) speciation and pyrite–Fe in CLASS drain sediments. Data points are means ± standard deviation of duplicate determinations. The concentrations for pyrite–Fe ($FeS_{2(s)}$–Fe) were estimated stoichiometrically from results for pyrite–S ($FeS_{2(s)}$–S).

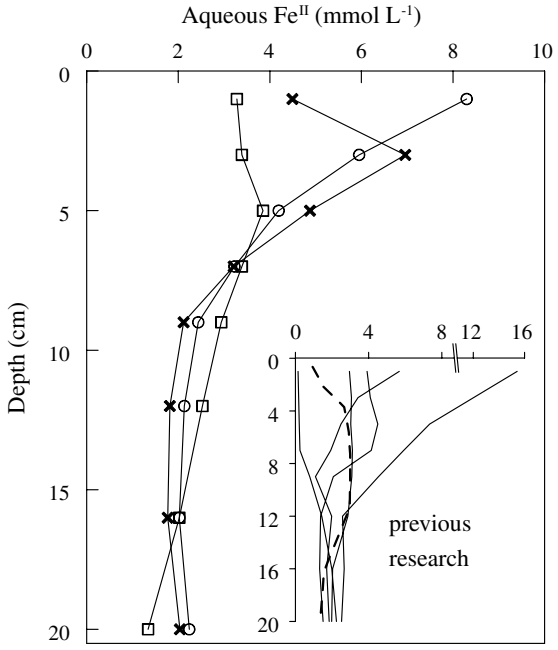

Fig. 8. Pore-water Fe^{II} in sediment profiles from site T (circles), site S (squares) and site B (crosses). The inset plot shows previously reported pore-water Fe^{II} data for CLASS drain sediments from Burton et al. (2006a) (solid lines) and Smith and Melville (2004) (broken line).

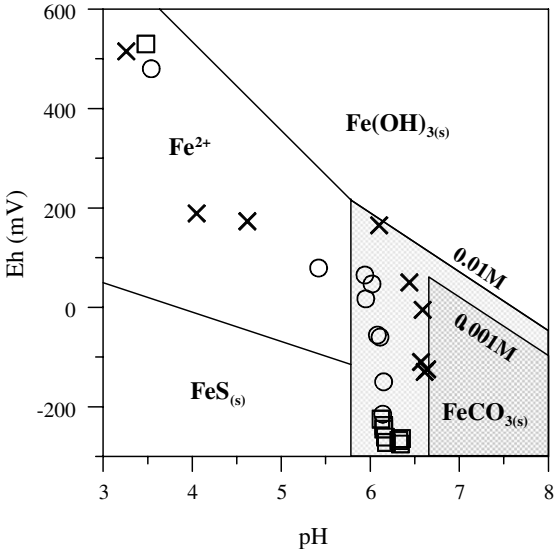

Fig. 9. Eh–pH data for samples at sites T (circles), S (squares) and B (crosses) showing stability fields for Fe^{2+}, $Fe(OH)_{3(s)}$ with $pK_{sp} = 38.5$, $FeS_{(s)}$ with $pK_{sp} = 2.95$, and $FeCO_{3(s)}$ with $pK_{sp} = 10.41$. The boundaries assume total dissolved Fe = 0.001 M, S = 0.001 M and HCO_3 = 0.001–0.01 M. The stability field for $FeCO_{3(s)}$ partially overlies the $FeS_{(s)}$ field to show potential controls on pore-water Fe^{2+} activity in the Fe-dominated sediments described in the present study.

oxalate-extractable Fe present at up to 2720 μmol g^{-1} at site T, 1460 μmol g^{-1} at site S and 956 μmol g^{-1} at site B (Fig. 11). Fig. 11 shows that most depth intervals exhibited high concentrations of both oxalate-extractable Fe(II) and Fe(III). However, the Fe(III)/Fe(II) ratio was generally greatest towards the sediment–water interface. This is consistent with the progressive reduction of Fe(III) as the former sediment surface becomes buried during sediment accretion.

The XRPD data provide conclusive evidence of abundant surficial (0–1 cm) schwertmannite at sites T and S

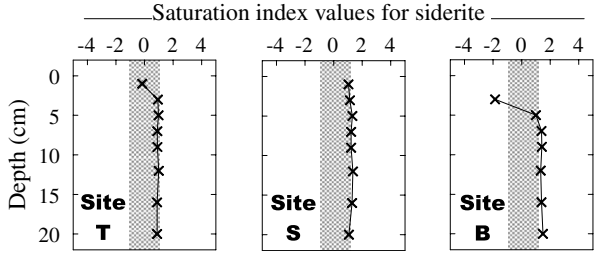

Fig. 10. Saturation index (*SI*) values for siderite based on aqueous speciation modeling of pore-water for sediment profiles from Sites T, S and B. The *SI* values for the 0–4 cm depth interval at site B were <-10 and are therefore not shown here. The shaded area shows the *SI* value range of -1 to $+1$.

(Fig. 4). Highly crystalline phases (mostly quartz and phyllosilicates) in sediment from site B make the XRPD identification of poorly ordered phases difficult (Bigham et al., 2002). Nevertheless, the surface-water Fe^{III} solubility and speciation calculations indicate that schwertmannite is probably also present at site B. Decreases in the abundance of oxalate-extractable Fe(III) with increasing sediment depth may therefore be due largely to reductive dissolution of schwertmannite (Regenspurg et al., 2004):

$$Fe_8O_8(OH)_6(SO_4)_{(s)} + 12H^+ + 2C_{Organic} \rightarrow 8Fe^{2+} + SO_4^{2-} + 2HCO_3^- + 8H_2O \quad (6)$$

The high pore-water Fe^{II} concentrations present in the 0–2 cm depth intervals support the importance of Eq. (6). This acidity-consuming process is likely to have contributed to pore-water pH in near-surface sediment being considerably higher than that of the overlying surface-water.

Schwertmannite is known to progressively transform to goethite (Bigham et al., 1996; Jonsson et al., 2005):

$$Fe_8O_8(OH)_6(SO_4)_{(s)} + 2H_2O \rightarrow 8FeOOH_{(s)} + 2H^+ + SO_4^{2-} \quad (7)$$

This transformation process is kinetically promoted by increased pH (Jonsson et al., 2005), which is caused by HCO_3-generating reactions such as SO_4-reduction (Eq. (2)) and Fe(III)-reduction (Eq. (6)) in the subsurface sediments described here. This is consistent with the XRPD data, which show the replacement of schwertmannite by goethite with increasing depth below the sediment water interface (Fig. 4). Examination of sub-surface sediment by SEM-EDX analysis revealed that material with an elemental composition consistent with goethite was present as rough-surfaced, spheroidal particles (Fig. 5c and d). This morphology is similar to spheroidal schwertmannite particles with "pin-cushion"-type surfaces present at the sediment surface. Such goethite pseudomorphs after schwertmannite have been observed previously in CLASS landscapes (Sullivan and Bush, 2004). This goethite

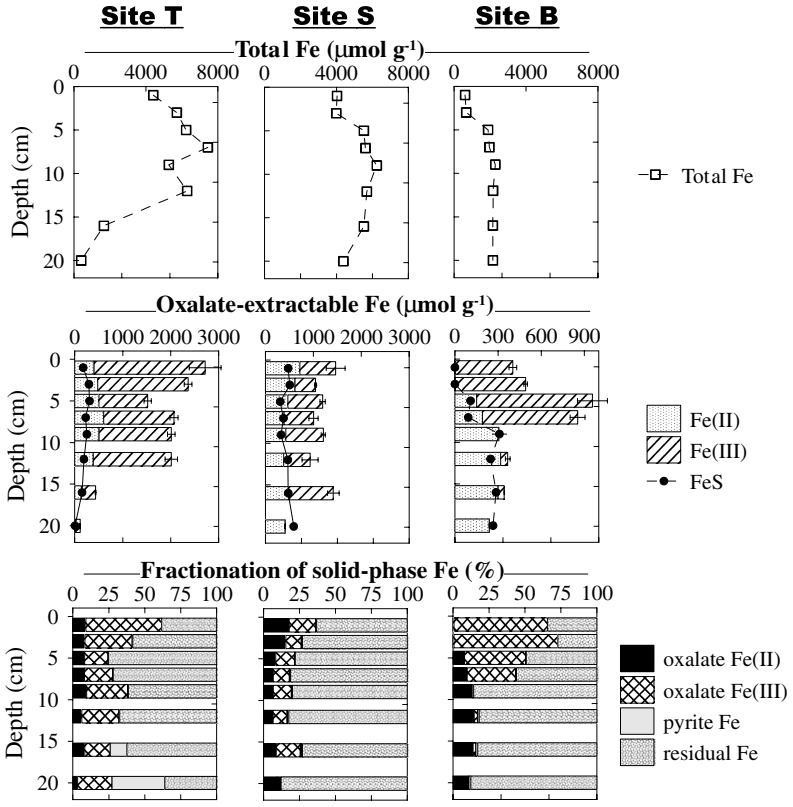

Fig. 11. Total Fe, oxalate-extractable Fe and fractionation of solid-phase Fe in sediment profiles from sites T, S and B. The FeS and pyrite Fe data were estimated stoichiometrically from the AVS and pyrite–S results, respectively (assuming AVS is 1:1 for Fe:S).

morphology supports the hypothesis that goethite formed via precursor schwertmannite, as described in Eq. (7).

Geochemical modeling discussed above indicates that the development of high pore-water Fe^{II} concentrations, derived from reductive dissolution of schwertmannite (Eq. (6)), may be regulated by siderite precipitation. The XRPD data for lower depth intervals at sites S and B show the presence of siderite (Fig. 4), in agreement with the stability-phase and *SI* value considerations (Figs. 10 and 11, respectively). Siderite was also identified by SEM-EDX as clusters of orthorhombic crystals associated with organic material (Fig. 5g, h and i). Overall, the data indicates that pore-water Fe^{II} solubility is primarily controlled by siderite precipitation/dissolution. This is significant as previous research has assumed that a sulfide phase, such as amorphous $FeS_{(s)}$, controls Fe solubility in sulfidic sediments from CLASS drains (Smith and Melville, 2004).

The pore-water data presented in Fig. 6 suggest that pore-water SO_4 is reduced to S^{-II} as the sediment is subjected to burial-induced anoxia. In the presence of abundant Fe^{II}, newly formed S^{-II} would be rapidly (<1 s) sequestered via $FeS_{(s)}$ precipitation (Rickard, 1995). Whilst the AVS concentrations were generally less than oxalate-extractable Fe(II), there was general agreement between depth trends for these two measures (Fig. 11). This observation, along with the very low pore-water S^{-II} concentrations indicates that AVS provided a reasonable measure of the abundance of $FeS_{(s)}$.

The XRPD data for lower depth intervals at sites T and S exhibit a broad peak at approximately 0.5 nm (i.e. 17°2θ) (Fig. 4). Herbert et al. (1998) report that XRPD data for Fe(II)/S(-II) solids precipitated in media containing SO_4-reducing bacteria also exhibit a broad, low intensity peak centred near 0.5 nm but lack other peaks characteristic of crystalline phases (e.g. mackinawite, greigite). Several laboratory-based studies of Fe–S behaviour have also attributed similar XRPD data to disordered mackinawite (Rickard, 1995; Wilkin and Barnes, 1996; Wolthers et al., 2003). Disordered mackinawite comprises sheets of Fe atoms linked in a tetrahedral coordination to four equidistant S atoms, with Van der Waals forces between S atoms holding the sheets together (Lennie et al., 1995). The characteristic broad XRPD peak at approximately 0.5 nm (i.e. 17°2θ) for disordered mackinawite derives from the inter-layer spacing of these Fe sheets (Rickard and Morse, 2005). According to Rickard (1995), disordered mackinawite forms within days of reaction between aqueous Fe^{II} and S^{-II} yielding an initial X-ray amorphous $FeS_{(s)}$ phase. The exact nature of the initial amorphous or disordered phase is poorly understood, yet up to 2 years is required for transformation to crystalline mackinawite (Rickard, 1995).

Examination of subsurface AVS-rich sediment by SEM-EDX revealed that material (identified by XRPD as disordered mackinawite) with stoichiometry spanning approx. $FeS_{0.9}$ to $FeS_{1.2}$ was present as surface coatings of convoluted platy crystals (Fig. 5e and f). This is similar to the morphology of an $FeS_{(s)}$ phase formed in a SO_4-reducing, reactive barrier for AMD treatment (Herbert et al., 2000). It is also comparable to material with an approximate 1:1 Fe:S stoichiometry present on the surface of pyrite framboids in CLASS (Bush and Sullivan, 2002). The XRPD, SEM-EDX and AVS data presented here provide strong evidence of the presence of abundant disordered mackinawite. This is significant as disordered mackinawite has been only rarely observed in natural marine or estuarine sediments (Rickard and Morse, 2005) and has not been previously identified in CLASS landscapes.

The co-existence of high concentrations of AVS (Fig. 7) and oxalate-extractable Fe(III) (Fig. 11) in several depth intervals suggests that S(−II)/Fe(III) interactions are highly likely. Such interactions may occur at the surface of goethite particles, which the XRPD data shows to co-exist with disordered mackinawite (Fig. 4). In this situation, S^{-II} can directly reduce solid-phase Fe(III) minerals producing Fe^{2+} and $S^0_{(s)}$ according to (Yao and Millero, 1996; Burton et al., 2006c):

$$2FeOOH_{(s)} + S^{-II} + 6H^+ \rightarrow S_{(s)}{}^0 + 2Fe^{2+} + 4H_2O \qquad (8)$$

The presence of $S_{(s)}{}^0$ at up to 218 μmol g^{-1} at site T, 286 μmol g^{-1} at site S and 101 μmol g^{-1} at site B reflects the importance of direct S(−II)/Fe(III) interactions (Fig. 7). The abundance of $S^0_{(s)}$ (as % of total RIS) was positively correlated with oxalate-extractable Fe(III) ($r = 0.550$; $P < 0.01$; $n = 24$). This correlation is consistent with previous work and indicates that $S^0_{(s)}$ forms in situ as a product of dynamic Fe–S redox cycling in CLASS waterway sediments (Burton et al., 2006c).

The formation of pyrite generally represents an important sink for reactive Fe species and thereby prevents accumulation of $FeS_{(s)}$ (e.g. Burton et al., 2006d). Pyrite formation has traditionally been viewed on the basis of limiting factors, specifically the availability of S, Fe and organic C (Berner, 1984). The very high concentrations of organic C (Fig. 6), AVS (Fig. 7) and pore-water Fe^{II} (Fig. 8) in the sediments described here demonstrate that these components were all readily available. SEM-EDX examination revealed that pyrite was present as both framboids and single crystals (Fig. 5j–o). However, in comparison to oxalate-extractable Fe(II) and Fe(III) (Fig. 11), pyrite–Fe was present at relatively low concentrations (7.3–148 μmol g^{-1} at site T, 154–294 μmol g^{-1} at site S and 0.8–28 μmol g^{-1} at site B; Fig. 7). As a consequence, pyrite–Fe generally comprised a relatively minor proportion of total Fe (Fig. 11).

Given that none of the usual limiting factors appear to be at low levels, the relatively low abundance of pyrite–Fe in the sediments described here is somewhat anomalous. The sediments may simply have had insufficient time for pyrite formation to sequester a substantial proportion of reactive Fe. This is based on the general assumption that formation of pyrite only occurs at very slow rates. However, Howarth (1979) observed significant in situ pyrite formation (verified by XRPD) within 2 days in salt marsh

sediments. Likewise, in situ radiotracer studies show that a substantial proportion of $^{35}S(-II)$, resulting from SO_4-reduction, precipitates as pyrite within hours of introducing trace amounts of $^{35}SO_4$ into anoxic sediments (Howarth and Merkel, 1984; Meier et al., 2004). Furthermore, Ritvo et al. (2003) found that reaction between S^{-II} and goethite surfaces at room temperature produced significant amounts of pyrite within 96 h. These studies clearly show that pyrite can form rapidly, which indicates that the relatively minor quantities of pyrite–Fe in the sediments described here warrants further examination.

Mechanistic data based on detailed kinetic investigations currently indicate that pyrite formation at ambient temperature occurs via either the polysulfide pathway (Rickard, 1975; Luther, 1991) or the hydrogen sulfide pathway (Rickard, 1997; Rickard and Luther, 1997). In the polysulfide pathway, $S^0_{(s)}$ produced via Eq. (8) reacts with pore-water S^{-II}, producing polysulfide ions ($S_{n+1}{}^{2-}$) which then react with $FeS_{(s)}$ to produce pyrite (Luther, 1991):

$$HS_{(aq)}{}^{-} + nS_{(s)}{}^{0} \rightarrow S_{(n+1)(aq)}{}^{2-} + H_{(aq)}{}^{+} \quad (9)$$

$$FeS_{(s)} + S_{n+1(aq)}{}^{2-} \rightarrow FeS_{2(s)} + S_{(n)(aq)}{}^{2-} \quad (10)$$

The rate of pyrite formation via this pathway is described by (Rickard, 1975):

$$\frac{d(FeS_{2(s)})}{dt} = k_1[FeS_{(s)}]^2[S_{8(s)}{}^{0}]\{S^{-II}\}\{H^+\} \quad (11)$$

where $[FeS_{(s)}]$ and $[S_{8(s)}{}^{0}]$ are the surface areas of $FeS_{(s)}$ and $S_{8(s)}{}^{0}$, $\{S^{-II}\}$ and $\{H^+\}$ denote the S^{-II} and H^+ activity, and k_1 is a rate constant equaling $\sim 10^{-12}$ cm^{-6} L mol^{-1} s^{-1} at 40 °C (Rickard, 1975).

The hydrogen sulfide pathway involves oxidation of $FeS_{(s)}$ by H_2S (Rickard and Luther, 1997):

$$FeS_{(s)} + H_2S_{(aq)} \rightarrow FeS_{2(s)} + H_{2(g)} \quad (12)$$

The rate of pyrite formation via this pathway is described by (Rickard, 1997):

$$\frac{d(FeS_{2(s)})}{dt} = k_2(FeS_{(s)})(H_2S_{(aq)}) \quad (13)$$

where $(FeS_{(s)})$ and $(H_2S_{(aq)})$ are the molar concentrations of $FeS_{(s)}$ and $H_2S_{(aq)}$, and k_2 is a rate constant equaling 1.03×10^{-4} L mol^{-1} s^{-1} at 25 °C (Rickard, 1997).

Eqs. (11) and (13) demonstrate that the rate of pyrite formation depends on the concentrations of $FeS_{(s)}$, $S^0_{8\ (s)}$ and S^{-II}. The results show that both $FeS_{(s)}$ and $S^0_{8\ (s)}$ were highly abundant (Fig. 7), whereas pore-water S^{-II} was undetectable in the sediments described here. These low pore-water S^{-II} concentrations therefore would be expected to cause kinetic retardation of $FeS_{(s)}$ conversion to pyrite. According to Eq. (3), the undetectable S^{-II} concentrations are attributable to the presence of very high concentrations of pore-water Fe^{II}. This effect of abundant Fe^{II} provides an explanation for both the accumulation of $FeS_{(s)}$ (as disordered mackinawite) and the anomalously low relative quantity of pyrite–Fe.

3.5. A geochemical model of sedimentary Fe transformations during sediment accretion in CLASS-associated waterways

Previous studies of sedimentary Fe dynamics in acidic waterways have focused on AMD-affected environments (Bigham et al., 1996; Peine et al., 2000; Meier et al., 2004; Regenspurg et al., 2004). However, sediments from AMD waterways typically contain only modest concentrations of labile organic C (Peine et al., 2000; Regenspurg et al., 2004). This contrasts greatly with organic-rich sediments found in drain waterways of CLASS landscapes (Bush et al., 2004b; Burton et al., 2006a). As a consequence, current conceptual models of sedimentary Fe behaviour in acidic waterways do not explain the trends in solubility and mineralogy for CLASS drain sediments. For example, the model developed by Peine et al. (2000) for AMD-affected lake sediments includes schwertmannite transformations and pyrite formation but does not consider siderite or disordered mackinawite. The present study shows that siderite and disordered mackinawite have a central role in sedimentary Fe cycling in CLASS drains. We therefore present a new conceptual model describing sedimentary Fe geochemistry during low-flow, accretionary periods in such waterways (Fig. 12).

During periods of dry weather, Fe enters the waterway study sites via influx of acidic groundwater from the adjacent oxidized, sulfuric, soil horizons (Figs. 2 and 12). Precipitation of schwertmannite (pathway A in Fig. 12), along with the death and decay of abundant aquatic

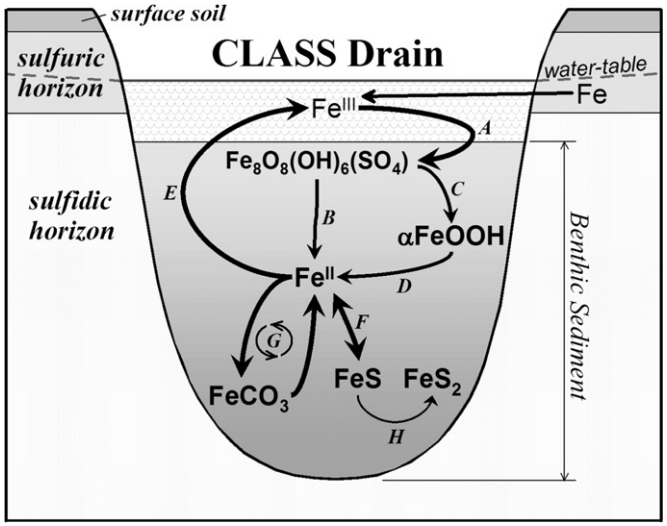

Fig. 12. Conceptual model of in situ Fe transformations in accreting CLASS drain sediments. (A) precipitation of schwertmannite ($Fe_8O_8(OH)_6(SO_4)$), (B) reductive dissolution of schwertmannite, (C) transformation of schwertmannite to goethite (αFeOOH), (D) reductive dissolution of goethite, (E) upward diffusion and oxidation of Fe^{II}, (F) precipitation–dissolution of disordered mackinawite (FeS), (G) regulation of pore-water Fe^{II} via precipitation–dissolution of siderite ($FeCO_3$), (H) and formation of pyrite (FeS_2; kinetically retarded due to high pore-water Fe^{II} concentrations).

vegetation contributes to sediment accretion. Degradation of abundant autochthonous organic C causes development of strongly reducing conditions below the sediment–water interface and leads to the reductive dissolution of schwertmannite (pathway B in Fig. 12). This process, along with HCO_3-promoted (i.e. pH-dependent) transformation of schwertmannite to goethite (pathway C in Fig. 12) and subsequent reductive dissolution of goethite (pathway D in Fig. 12), is a major contributor to the development of very high pore-water Fe^{II} concentrations. Upward diffusion of Fe^{II} across the sediment–water interface and subsequent oxidation re-supplies surface-water Fe^{III} (pathway E in Fig. 12).

Microbial degradation of organic matter in these sediments facilitates the accumulation of high concentrations of HCO_3 and the development of near-neutral pore-water pH. This also promotes SO_4-reduction, which becomes important in Fe-rich sediments at $pH > 5.5$ (Fortin et al., 1996). The accumulation of disordered mackinawite (pathway F in Fig. 12) is the result of SO_4-reduction and the reaction between the produced S^{-II} and pore-water Fe^{II}.

Although disordered mackinawite is highly abundant and indicative of active SO_4-reduction, the sediments contain insufficient pore-water S^{-II} for precipitation of disordered mackinawite to limit the accumulation of pore-water Fe^{II}. Rather in the HCO_3-rich sediments described here, siderite precipitation-dissolution regulates the pore-water Fe^{II} concentrations (pathway G in Fig. 12). The presence both of siderite and disordered mackinawite is of interest as there are few reports of the co-existence of Fe(II) carbonate and sulfide minerals in sediments (Pye et al., 1990). Although unusual, Pye et al. (1990) hypothesize that simultaneous accumulation of both siderite and iron monosulfides (e.g. disordered mackinawite) may occur where the rate of Fe(III) reduction exceeds SO_4 reduction. This situation is likely to occur as result of the ample supply of reactive Fe(III) (i.e. schwertmannite) in accretionary CLASS drain sediments.

Disordered mackinawite is assumed to contribute to sedimentary AVS, yet has been rarely observed in natural sulfidic sediments (Rickard and Morse, 2005). The present study shows for the first time that disordered mackinawite is a major component of sedimentary AVS in CLASS drains. Acid-volatile sulfide (AVS) is typically present at low levels in natural estuarine and marine sediments (Morse and Cornwell, 1987), with accumulation being limited by its generally efficient conversion to pyrite (Morse and Rickard, 2004). However, pyrite–Fe does not account for a significant fraction of sedimentary Fe in CLASS drains. This is because the rate of pyrite formation (pathway H in Fig. 12) is very slow at low concentrations of pore-water S^{-II} (which is maintained at low concentrations by the very high Fe^{II} concentrations). Therefore, high pore-water Fe^{II} concentrations in CLASS drain sediments contribute to accumulation of siderite and disordered mackinawite at the expense of pyrite–Fe.

4. Conclusions

We employed selective extractions, geochemical modeling, XRPD and SEM-EDX to describe sedimentary Fe behaviour in acidic CLASS drains. These waterways receive inputs of acid sulfate groundwater and are therefore analogous to streams and lakes affected by AMD. Like many AMD settings, schwertmannite precipitation in CLASS drains contributes to the formation of Fe(III)-rich benthic sediments. However unlike AMD waterways, CLASS drain sediments contain abundant labile organic material which drives the development of anoxic, near-neutral conditions below the sediment water interface. The burial and prolonged exposure of schwertmannite-rich sediment to these conditions results in (1) schwertmannite conversion to goethite, (2) reductive dissolution of schwertmannite and goethite, (3) SO_4-reduction, (4) formation of anomalously high AVS concentrations, (5) co-existence of siderite and disordered mackinawite, and (6) retarded rates for conversion of disordered mackinawite to pyrite.

Acknowledgments

We thank Maxine Dawes for assistance with the SEM-EDX analyses, which were conducted in the SEM Facilities at Southern Cross University. Associate Editor John W. Morse, Christopher H. Gammons and three anonymous reviewers provided constructive comments on an earlier draft of this manuscript. This research was funded by the Australian Commonwealth Government through an Australian Research Council grant (DP0453280 ''Contemporary sulfur biomineralisation in acid sulfate soil landscapes'').

Associate editor: John W. Morse

References

Amirbahman, A., Schonenberger, R., Johnson, C.A., Sigg, L., 1998. Aqueous- and solid biogeochemistry of a calcareous aquifer system downgradient from a municipal solid waste landfill (Winterhur, Switzerland). *Environ. Sci. Technol.* **32**, 1933–1940.

APHA (1998) *Standard Methods for the Examination of Water and Wastewater*. (20th ed.) American Public Health Association–American Water Works Association. Baltimore, USA.

Astrom, M., Spiro, B., 2000. Impact of isostatic uplift and ditching of sulfidic sediments on the hydrochemistry of major and trace elements and sulfur isotope ratios in streams, Western Finland. *Environ. Sci. Technol.* **34**, 1182–1188.

Berner, R.A., 1984. Sedimentary pyrite formation: an update. *Geochim. Cosmochim. Acta* **48**, 605–615.

Bigham, J.M., Nordstrom, D.K., 2000. Iron and aluminium hydroxysulfates from acid sulfate waters. In: Alpers, C.N., Jambor, J.L., Nordstrom, D.K. (Eds.), *Sulfate Minerals–Crystallography, Geochemistry and Environmental Significance*, *Rev. Miner. Geochem.*, vol. 40. Mineral. Soc. Am., Washington, DC, pp. 351–403.

Bigham, J.M., Schwertmann, U., Carlson, L., Murad, E., 1990. A poorly crystallized oxyhydroxysulfate of iron formed by bacterial oxidation of Fe(II) in acid mine waters. *Geochim. Cosmochim. Acta* **54**, 2743–2758.

Bigham, J.M., Schwertmann, U., Traina, S.J., Winland, R.L., Wolf, M., 1996. Schwertmannite and the chemical modeling of iron in acid sulfate waters. *Geochim. Cosmochim. Acta* **60**, 2111–2121.

Bigham, J.M., Fitzpatrick, R.W., Schulze, D.G., 2002. Iron oxides. In: Dixon, J.B., Schulze, D.G., Daniels, W.L. (Eds.), *Soil Mineralogy with Environmental Applications*. Soil Science Society of America, Madison, WI.

Bjerg, P.L., Rugge, K., Pedersen, J.K., Christensen, T.H., 1995. Distribution of redox-sensitive groundwater quality parameters downgradient of a landfill (Grinsted, Denmark). *Environ. Sci. Technol.* **29**, 1387–1394.

Burton, E.D., Phillips, I.R., Hawker, D.W., 2005. Reactive sulfide relationships with trace metal extractability in sediments from southern Moreton Bay, Australia. *Mar. Pollut. Bull.* **50**, 583–608.

Burton, E.D., Bush, R.T., Sullivan, L.A., 2006a. Reduced inorganic sulfur speciation in drain sediments from acid-sulfate soil landscapes. *Environ. Sci. Technol.* **40**, 888–893.

Burton, E.D., Bush, R.T., Sullivan, L.A., 2006b. Acid-volatile sulfide oxidation in coastal floodplain drains: iron–sulfur cycling and effects on water quality. *Environ. Sci. Technol.* **40**, 1217–1222.

Burton, E.D., Bush, R.T., Sullivan, L.A., 2006c. Elemental sulfur in drain sediments associated with acid sulfate soils. *Appl. Geochem.* **21**, 1240–1247.

Burton, E.D., Bush, R.T., Sullivan, L.A., 2006d. Fractionation and extractability of sulfur, iron and trace elements in sulfidic sediments. *Chemosphere* **64**, 1421–1428.

Bush, R.T., Sullivan, L.A., 1997. Morphology and behaviour of greigite from a Holocene sediment in Eastern Australia. *Aust. J. Soil Res.* **35**, 853–861.

Bush, R.T., Sullivan, L.A., 1999. Pyrite micromorphology in three Australian Holocene sediments. *Aust. J. Soil Res.* **37**, 637–653.

Bush, R.T., Sullivan, L.A., 2002. Pyrite formation in estuarine sediments of eastern Australia. In: Lin, C., Melville, M.D., Sullivan, L.A. (Eds.), *Acid sulfate soils in Australia and China*. Science Press, Beijing, China.

Bush, R.T., McGrath, R., Sullivan, L.A., 2004a. Occurrence of marcasite in an organic-rich Holocene estuarine mud. *Aust. J. Soil Res.* **42**, 617–621.

Bush, R.T., Fyfe, D., Sullivan, L.A., 2004b. Occurrence and abundance of monosulfidic black ooze in coastal acid sulfate soil landscapes. *Aust. J. Soil Res.* **42**, 609–616.

Bush, R.T., Sullivan, L., Fyfe, D., Johnston, S.J., 2004c. Redistribution of monosulfidic black oozes by floodwaters in a coastal acid sulfate soil floodplain. *Aust. J. Soil Res.* **42**, 603–607.

Canfield, D.E., Thamdrup, B., Hansen, J.W., 1993. The anerobic degradation of organic matter in Danish coastal sediments: iron reduction, manganese reduction and sulfate reduction. *Geochim. Cosmochim. Acta* **57**, 3867–3883.

Dent, D.L., 1986. *Acid Sulphate Soils: A Baseline for Research and Development*. (International Institute for Land Reclamation and Improvement; Netherlands).

Dent, D.L., 2000. An international perspective. In: Ahern, C.R., Hey, K.M., Watling, K.M., Eldershaw, V.J. (Eds.), *Acid Sulfate Soils: Environmental Issues, Assessment and Management*. Queensland Department of Natural Resources, Brisbane, pp. 12,1–12,4.

Fanning, D.S., Rabenhorst, M.C., Burch, S.N., Islam, K.R., Tangren, S.A., 2002. Sulfides and sulfates. In: Dixon, J.B., Schulze, D.G., Daniels, W.L. (Eds.), *Soil Mineralogy with Environmental Applications*. Soil Science Society of America, Madison, WI.

Fortin, D., Davis, B., Beveridge, T.J., 1996. The role of *Thiobacillus* and sulfate-reducing bacteria in iron biocycling in oxic and acidic mine tailings. *FEMS Microbiol. Ecol.* **21**, 11–24.

Gammons, C.H., Nimick, D.A., Parker, S.R., Cleasby, T.E., McCleskey, R.B., 2005. Diel behaviour of iron and other heavy metals in a mountain stream with acidic to neutral pH: Fisher Creek, Montana, USA. *Geochim. Cosmochim. Acta* **69**, 2505–2516.

Herbert, R.B., Benner, S.G., Pratt, A.R., Blowes, D.W., 1998. Surface chemistry and morphology of poorly crystalline iron sulfides precipitated in media containing sulfate-reducing bacteria. *Chem. Geol.* **144**, 87–97.

Herbert, R.B., Benner, S.G., Blowes, D.W., 2000. Solid phase iron–sulfur geochemistry of a reactive barrier for treatment of mine drainage. *Appl. Geochem.* **15**, 1331–1343.

Howarth, R.W., 1979. Pyrite: its rapid formation in a salt marsh and its importance in ecosystem metabolism. *Science* **203**, 49–51.

Howarth, R.W., Merkel, S., 1984. Pyrite formation and the measurement of sulfate reduction in salt marsh sediments. *Limnol. Oceanogr.* **29**, 598–608.

Hsieh, Y.P., Chung, S.W., Tsau, Y.J., Sue, C.T., 2002. Analysis of sulfides in the presence of ferric minerals by diffusion methods. *Chem. Geol.* **182**, 195–201.

Ingvorsen, K., Zehnder, A.J.B., Jørgensen, B.B., 1984. Kinetics of sulfate and acetate uptake by *Desulfobacter postgatei*. *Appl. Environ. Microbiol.* **47**, 403–408.

Jakobsen, R., Postma, D., 1999. Redox zoning, rates of sulfate reduction and interactions with Fe-reduction and methanogenesis in a shallow sandy aquifer, Romo, Denmark. *Geochim. Cosmochim. Acta* **63**, 137–151.

Jensen, D.L., Boddum, J.K., Tjell, J.C., Christensen, T.H., 2002. The solubility of rhodochrosite ($MnCO_3$) and siderite ($FeCO_3$) in anaerobic aquatic environments. *Appl. Geochem.* **17**, 503–511.

Johnston, S.G., Slavich, P.G., Hirst, P., 2004. The acid flux dynamics of two artificial drains in acid sulfate soil backswamps on the Clarence River floodplain, Australia. *Aust. J. Soil Res.* **42**, 623–637.

Jonsson, J., Persson, P., Sjoberg, S., Lovgren, L., 2005. Schwertmannite precipitated from acid mine drainage: phase transformation, sulphate release and surface properties. *Appl. Geochem.* **20**, 179–191.

Kinsela, A.S., Melville, M.D., 2004. Mechanisms of acid sulfate soil oxidation and leaching under sugarcane cropping. *Aust. J. Soil Res.* **42**, 569–578.

Langmuir, D., 1997. *Aqueous Environmental Geochemistry*. Prentice-Hall Publishers, New Jersey, USA.

Lennie, A.R., Redfern, S.A.T., Schofield, P.F., Vaughan, D.J., 1995. Synthesis and Rietveld crystal structure refinement of mackinawite, tetragonal FeS. *Mineral. Mag.* **59**, 677–683.

Lovley, D.R., 1997. Microbial Fe(III) reduction in subsurface environments. *FEMS Microbiol. Rev.* **20**, 305–313.

Luther, G.W., 1991. Pyrite synthesis via polysulfide compounds. *Geochim. Cosmochim. Acta* **55**, 2839–2849.

Luther, G.W., Kostka, J.E., Church, T.M., Sulzberger, B., Stumm, W., 1992. Seasonal iron chemistry in the salt–marsh sedimentary environment: the importance of ligand complexes with Fe(II) and Fe(III) in the dissolution of Fe(III) minerals and pyrite, respectively. *Mar. Chem.* **40**, 81–103.

Macdonald, B.C.T., Smith, J., Keene, A.F., Tunks, M., Kinsela, A., White, I., 2004. Impacts of runoff from sulfuric soils on sediment chemistry in an estuarine lake. *Sci. Total Environ.* **329**, 115–130.

Majzlan, J., Navrotsky, A., Schwertmann, U., 2004. Thermodynamics of iron oxides: Part III. Enthalpies of formation and stability of ferrihydrite ($\sim Fe(OH)_3$), schwertmannite ($\sim FeO(OH)_{3/4}(SO_4)_{1/8}$), and ε-Fe_2O_3. *Geochim. Cosmochim. Acta* **68**, 1049–1059.

Majzlan, J., Myneni, S.C.B., 2005. Speciation of iron and sulfate in acid waters: aqueous clusters to mineral precipitates. *Environ. Sci. Technol.* **39**, 188–194.

Meier, J., Babenzien, H.D., Wendt-Potthoff, K., 2004. Microbial cycling of iron and sulfur in sediments of acidic and pH-neutral mining lakes in Lusatia (Brandenberg, Germany). *Biogeochemistry* **67**, 135–156.

Morse, J.W., Cornwell, J.C., 1987. Analysis and distribution of iron sulfide minerals in recent anoxic marine sediments. *Mar. Chem.* **22**, 55–69.

Morse, J.W., Millero, F.J., Cornwell, J.C., Rickard, D., 1987. The chemistry of the hydrogen sulfide and iron sulfide systems in natural waters. *Earth Sci. Rev.* **24**, 1–42.

Morse, J.W., Rickard, D., 2004. Chemical dynamics of sedimentary acid volatile sulfide. *Environ. Sci. Technol.* **38**, 131A–136A.

Neumann, T., Rausch, N., Leipe, T., Dellwig, O., Berner, Z., Bottcher, M.E., 2005. Intense pyrite formation under low-sulfate conditions in

the Achterwasser lagoon, SW Baltic Sea. *Geochim. Cosmochim. Acta* **69**, 3619–3630.

Parkhurst, D.L., Appelo, C.A.J., 1999. *User's Guide to PHREEQC (Version 2)–A Computer Program for Speciation, Batch-reaction, One-dimensional Transport, and Inverse Geochemical Calculations*. Water resources investigations report 99-4259, US Geological Survey, Denver, Colorado.

Peine, A., Tritschler, A., Kusel, K., Peiffer, S., 2000. Electron flow in iron-rich acidic sediment—evidence for an acidity driven iron cycle. *Limnol. Oceanogr.* **45**, 1077–1087.

Phillips, E.J.P., Lovley, D.R., 1987. Determination of Fe(III) and Fe(II) in oxalate extracts of sediments. *Soil Sci. Soc. Am. J.* **51**, 938–941.

Postma, D., 1982. Pyrite and siderite formation in brackish and freshwater swamp sediments. *Am. J. Sci.* **282**, 1151–1183.

Pye, K., Dickson, J.A.D., Schiavon, N., Coleman, M.L., Cox, M., 1990. Formation of siderite–Mg–calcite–iron sulphide concretions in intertidal marsh and sandflat sediments, north Norfolk, England. *Sedimentology* **37**, 325–343.

Regenspurg, S., Brand, A., Peiffer, S., 2004. Formation and stability of schwertmannite in acidic mining lakes. *Geochim. Cosmochim. Acta* **68**, 1185–1197.

Rickard, D.T., 1975. Kinetics and mechanisms of pyrite formation at low temperatures. *Am. J. Sci.* **275**, 636–652.

Rickard, D.T., 1995. Kinetics of FeS precipitation, Part 1: competing reaction mechanisms. *Geochim. Cosmochim. Acta* **59**, 4367–4379.

Rickard, D., 1997. Kinetics of pyrite formation by the H_2S oxidation of iron (II) monosulfide in aqueous solutions between 25 and 125 °C: the rate equation. *Geochim. Cosmochim. Acta* **61**, 115–134.

Rickard, D., Luther, G.W., 1997. Kinetics of pyrite formation by the H_2S oxidation of iron (II) monosulfide in aqueous solutions between 25 and 125 °C: the mechanism. *Geochim. Cosmochim. Acta* **61**, 135–147.

Rickard, D., Morse, J.W., 2005. Acid volatile sulfide (AVS). *Mar. Chem.* **97**, 141–197.

Ritvo, G., White, G.N., Dixon, J.B., 2003. A new iron sulfide precipitated from saline solutions. *Soil Sci. Soc. Am. J.* **67**, 1303–1308.

Sammut, J., White, I., Melville, M.D., 1996. Acidification of an estuarine tributary in eastern Australia due to drainage of acid sulfate soils. *Mar. Freshwater Res.* **47**, 669–684.

Smith, J., Melville, M.D., 2004. Iron monosulfide formation and oxidation in drain-bottom sediments of an acid sulfate soil environment. *Appl. Geochem.* **19**, 1837–1853.

Stumm, W., Morgan, J.J., 1996. *Aquatic Chemistry*, third ed. John Wiley & Sons, New York.

Sullivan, L.A., Bush, R.T., 1997. Quantitative microanalysis of rough soil surfaces in the scanning electron microscope using a peak-to-background method. *Soil Sci.* **162**, 749–757.

Sullivan, L.A., Bush, R.T., McConchie, D.M., 2000. A modified chromium-reducible sulfur method for reduced inorganic sulfur: optimum reaction time for acid sulfate soil. *Aust. J. Soil Res.* **38**, 729–734.

Sullivan, L.A., Bush, R.T., 2000. The behaviour of drain sludge in acid sulfate soil areas: some implications for acidification of waterways and drain maintenance. In: Slavich, P. (Eds.) *Proceedings of workshop on remediation of broadacre acid sulfate soils*. Acid Sulfate Soil Management Advisory Committee, Australia, pp. 43–49.

Sullivan, L.A., Bush, R.T., Fyfe, D., 2002. Acid sulfate soil drain ooze: distribution, behaviour and implications for acidification and deoxygenation of waterways. In: Lin, C., Melville, M.D., Sullivan, L.A. (Eds.), *Acid Sulfate Soils in Australia and China*. Science Press, Beijing, pp. 91–99.

Sullivan, L.A., Bush, R.T., 2004. Iron precipitate accumulations associated with waterways in drained coastal acid sulfate landscapes of eastern Australia. *Mar. Freshwater Res.* **55**, 727–736.

van Breemen, N., 1982. Genesis, morphology, and classification of acid sulfate soils in coastal plains. In: Kittrick, J.A., Fanning, D.S., Hossner, L.R. (Eds.), *Acid Sulfate Weathering*, vol. 10. SSSA Special Publication, Madison, Wisconsin, USA, pp. 95–108.

Ward, N.J., Sullivan, L.A., Fyfe, D.M., Bush, R.T., Ferguson, A.J.P., 2004. The process of sulfide oxidation in some acid sulfate soil materials. *Aust. J. Soil Res.* **42**, 449–458.

Wieder, R.K., Lang, G.E., Granus, V.A., 1985. An evaluation of wet chemical methods for quantifying sulfur fractions in freshwater wetland peat. *Limnol. Oceanogr.* **30**, 1109–1115.

Wilkin, R.T., Barnes, H.L., 1996. Pyrite formation by reactions of iron monosulphides with dissolved inorganic and organic sulphur species. *Geochim. Cosmochim. Acta* **60**, 4167–4179.

Wilson, B.P., White, I., Melville, M.D., 1999. Floodplain hydrology, acid discharge and change in water quality associated with a drained acid sulphate soil. *Mar. Freshwater Res.* **50**, 149–157.

Wolthers, M., Van der Gaast, S.J., Rickard, D., 2003. The structure of disordered mackinawite. *Am. Mineral.* **88**, 2007–2015.

Yao, W., Millero, F.J., 1996. Oxidation of hydrogen sulfide by hydrous Fe(III) oxides in seawater. *Mar. Chem.* **52**, 1–16.